Improving the Robustness of a Surface Integral Formulation for Wideband Impedance Extraction of 3D Structures *

Zhenhai Zhu †, Jingfang Huang *, Ben Song †, Jacob White †

† Department of Electrical Engineering and Computer Science
Massachusetts Institute of Technology, Cambridge, MA 02139
{zhzhu, bensong, white}@rle-vlsi.mit.edu
* Department of Mathematics
University of North Carolina, Chapel Hill, NC 27599
huang@amath.unc.edu

Abstract

In order for parasitic extraction of high-speed integrated circuit interconnect to be sufficiently efficient, and fit with model-order reduction techniques, a robust wideband surface integral formulation is essential. One recently developed surface integral formulation has shown promise, but was plagued with numerical difficulties of poorly understood origin. In this paper we show that one of that formulation's difficulties was related to the inaccuracy in the approach to evaluate integrals over discretization panels, and we present an accurate approach based on an adapted piecewise quadrature scheme. We also show that the condition number of the original system of integral equations can be reduced by differentiating one of the integral equations. Computational results on a ring and a spiral inductor are used to show that the new quadrature scheme and the differentiated integral formulation improve accuracy and accelerate the convergence of iterative solution methods.

1. Introduction

The layout parasitics in critical nets in high frequency analog and high speed digital integrated circuits must be analyzed using methods that take into account distributed resistive, capacitive and inductive effects, and may even require a careful treatment of radiation. The only approaches that have proven to be capable of detailed electromagnetic analysis of complicated integrated circuit interconnect are the accelerated integral equation methods like those used in FastCap [1] and FastHenry [2]. In addition, it is widely agreed that the integral formulation used must be a surface formulation, as such formulations avoid a frequency-dependent discretization of the interior of conductors and the substrate [3, 4].

One recently developed surface integral formulation has shown promise [3], but was plagued with numerical difficulties of poorly understood origin. In this paper we show that one of that formulation's difficulties was related to inaccuracy in the approach to evaluate integrals over discretization panels, and we present an accurate approach based on an adapted piecewise quadrature scheme. We also show that the condition number of the original system of integral equations can be reduced by differentiating one of the integral equations. Computational results on a ring and a spiral inductor are used to show that the new quadrature scheme and the differentiated integral formulation improve accuracy and accelerate the convergence of iterative solution methods.

*This work was sponsored by the Semiconductor Research Corporation, the NSF program in computer-aided design, and grants from Synopsys, Compaq and Intel.

2. Surface Formulation

The surface integral formualtion proposed in [3, 4] is as follows

$$\int_{S_k} d\vec{r'} G_1(\vec{r},\vec{r'}) \frac{\partial \vec{E}(\vec{r'})}{\partial n(\vec{r'})} - \int_{S_k} d\vec{r'} \frac{\partial G_1(\vec{r},\vec{r'})}{\partial n(\vec{r'})} \vec{E}(\vec{r'}) = \frac{1}{2}\vec{E}(\vec{r}) \tag{1}$$

$$\int_{S} d\vec{r'} G_0(\vec{r},\vec{r'}) \frac{\partial \vec{E}(\vec{r'})}{\partial n(\vec{r'})} - \int_{S} d\vec{r'} \frac{\partial G_0(\vec{r},\vec{r'})}{\partial n(\vec{r'})} \vec{E}(\vec{r'}) + \nabla\phi(\vec{r}) = -\frac{1}{2}\vec{E}(\vec{r}) \tag{2}$$

$$\int_{S} d\vec{r'} G_0(\vec{r},\vec{r'}) \rho_s(\vec{r'}) = \varepsilon\phi(\vec{r}) \tag{3}$$

$$\nabla \cdot \vec{E}(\vec{r}) = 0 \tag{4}$$

$$\hat{n} \cdot \vec{E}(\vec{r}) = \frac{i\omega\rho_s(\vec{r})}{\sigma},\ \vec{r} \in S_k \tag{5}$$

where S_k is the surface of the k-th conductor, S is the union of the S_k's, $\vec{r}$ and $\vec{r'}$ are on S, ρ_s denotes the surface charge density, E is the electric field, σ is the conductivity of the conductor, $\hat{n}$ is the outward normal unit vector on the conductor surface, and

$$G_1(\vec{r},\vec{r'}) = \frac{e^{ik_1|\vec{r}-\vec{r'}|}}{4\pi|\vec{r}-\vec{r'}|},\ k_1 = \sqrt{\omega^2\varepsilon\mu - i\omega\mu\sigma}\ , \tag{6}$$

$$G_0(\vec{r},\vec{r'}) = \frac{e^{ik_0|\vec{r}-\vec{r'}|}}{4\pi|\vec{r}-\vec{r'}|},\ k_0 = \omega\sqrt{\varepsilon\mu}\ , \tag{7}$$

where ω is the excitation frequency, and ε and μ are the dielectric permittivity and magnetic permeability, respectively. It should be noted that the jump condition of the double-layer integral has already been applied in (1) and (2). The formulation has eight scalar state variables, E_x, E_y, E_z, $\frac{\partial Ex}{\partial n}$, $\frac{\partial Ey}{\partial n}$, $\frac{\partial Ez}{\partial n}$, ϕ and ρ_s. Since the equation (2) along the normal direction is not enforced, the total number of scalar equations is also eight.

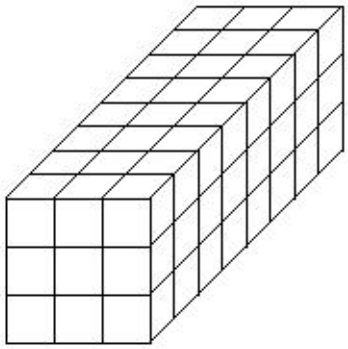

Figure 1: Panel discretization

3. Panel Integration

In order to discretize the system of integral equations (1–5), a piecewise-constant centroid collocation scheme is used. The conductor surface is discretized into N flat quadrilateral panels. Seven unknowns are associated with each panel: E_x, E_y, E_z, $\frac{\partial Ex}{\partial n}$, $\frac{\partial Ey}{\partial n}$, $\frac{\partial Ez}{\partial n}$ and ρ_s. The scalar potential ϕ is associated with the panel vertices. For more details about the discretization, please refer to [3].

3.1 Definition

After discretization, the integrals over conductor surface S or S_k are replaced by the summation of integrals over panels. These integrals are

$$I_1(\vec{r}) = \int_{P_i} d\vec{r'} G(\vec{r},\vec{r'}) \tag{8}$$

$$I_2(\vec{r}) = \int_{P_i} d\vec{r'} \frac{\partial G(\vec{r},\vec{r'})}{\partial n(\vec{r'})} = \hat{n}(P_i) \cdot \int_{P_i} d\vec{r'} \nabla_{\vec{r'}} G(\vec{r},\vec{r'}) \tag{9}$$

$$I_3(\vec{r}) = \frac{\partial}{\partial n(\vec{r})} \int_{P_i} d\vec{r'} G(\vec{r},\vec{r'}) = \hat{n}(\vec{r}) \cdot \nabla_{\vec{r}} \int_{P_i} d\vec{r'} G(\vec{r},\vec{r'}) \tag{10}$$

where P_i is the i-th panel, $\hat{n}(P_i)$ is the unit normal vector on the flat panel P_i, and $G(\vec{r},\vec{r'})$ is either $G_0(\vec{r},\vec{r'})$ or $G_1(\vec{r},\vec{r'})$ defined in (6) and (7). From the symmetry property of the Green's function, it follows that

$$\int_{P_i} d\vec{r'} \nabla_{\vec{r'}} G(\vec{r},\vec{r'}) = -\nabla_{\vec{r}} \int_{P_i} d\vec{r'} G(\vec{r},\vec{r'}) = -\nabla_{\vec{r}} I_1(\vec{r}). \tag{11}$$

Therefore, to compute the integrals in equation (8) (9) and (10), all we need is to compute $I_1(\vec{r})$ and $\frac{\partial I_1(\vec{r})}{\partial D}$, where D stands for x, y or z.

3.2 Decomposition

It is shown in [5] that any integration over a polygon is equal to the signed summation of the integration over a chosen set of triangles. The vertices of these triangles are those of the polygon and the projection of the evaluation point onto the plane where the polygon lies, as shown in figure 2. To be more precise, let $f(\vec{r})$ be a general integrand, its integration over a polygon in figure 2 could be written as

$$\int_S d\vec{r} f(\vec{r}) = \sum_{i=1}^{N} s_i \int_{PV_iV_{i+1}} d\vec{r} f(\vec{r}) \tag{12}$$

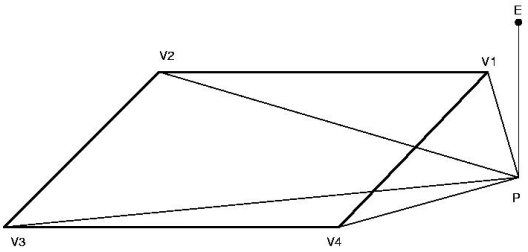

Figure 2: Decomposition of an integration over a polygon into several integrations over traingels

where N is the number of vertices, $V_{N+1} = V_1$, and $s_i = -1$ if V_iV_{i+1} is clockwise looking from the evaluation point E and $s_i = 1$ if otherwise. This idea was used in [4] to compute the integrals $I_1(\vec{r})$ and $\frac{\partial I_1(\vec{r})}{\partial D}$.

3.3 Desingularization and Reduction to 1-D integration

In a polar coordinate system, a triangle after the decomposition is shown in figure 3. Using the relation $R = \sqrt{r^2+h^2}$ and $RdR = rdr$, the integrals I_1 and $\frac{\partial I_1}{\partial D}$ over this triangle could be rewritten in polar coordinates as

$$\begin{aligned} I_1 &= \int_{\theta_A}^{\theta_B} d\theta \int_0^{r_1(\theta)} rdr \frac{e^{ikR}}{4\pi R} \\ &= \int_{\theta_A}^{\theta_B} d\theta \int_h^{R_1(\theta)} dR \frac{e^{ikR}}{4\pi} \\ &= \int_{\theta_A}^{\theta_B} d\theta \frac{e^{ikR_1(\theta)} - e^{ikh}}{4\pi ik} \quad k \neq 0 \end{aligned} \tag{13}$$

$$or \quad = \int_{\theta_A}^{\theta_B} d\theta \frac{R_1(\theta) - h}{4\pi} \quad k = 0 \tag{14}$$

$$\frac{\partial I_1}{\partial D} = \int_{\theta_A}^{\theta_B} d\theta \left(\frac{e^{ikR_1(\theta)}}{4\pi} \frac{\partial R_1(\theta)}{\partial D} - \frac{e^{ikh}}{4\pi} \frac{\partial h}{\partial D}\right) \tag{15}$$

Now the singularity of the original kernels in I_1 and $\frac{\partial I_1}{\partial D}$ has been eliminated and the 2-D integrations have been reduced to 1-D integrations. The quadrature rule is used to compute the two 1-D integrations in equation (13) and (15). The shared rapid changing kernel in these two integrals is $f(\theta) = e^{ikR_1(\theta)}$, where $R_1(\theta) = \sqrt{d^2 sec^2(\theta) + h^2}$. When $d << AB$, $\theta_A \approx \frac{-\pi}{2}$ and $\theta_B \approx \frac{\pi}{2}$, and $f(\theta)$ changes rapidly over the interval. Many quadrature points must be used to achieve reasonable accuracy.

3.4 Piece-wise Quadrature Scheme

A simple variable transformation and a piece-wise quadrature scheme can be used to solve the above-mentioned problem. Let $x = dtan(\theta)$, it easily follows that $\frac{d\theta}{dx} = \frac{d}{r^2}$, where $r^2 = d^2 + x^2$. The rapidly changing part of I_1 and $\frac{\partial I_1}{\partial D}$ could be rewritten as

$$\int_{\theta_A}^{\theta_B} d\theta e^{ikR} = \int_{x_A}^{x_B} dx g(x), where\ g(x) = \frac{d}{r^2} e^{ik\sqrt{h^2+r^2}} \tag{16}$$

The distribution of the integrand $g(x)$ is shown in the top figure of the figure 4. Many quadrature points must still be used to get accurate evaluation because of the rapid variation about $x = 0$. However if we divide the integration domain into two sub-domains, as shown in the middle and the bottom figure of the figure 4, and use a piece-wise integration scheme, the number of quadrature points needed will be dramatically

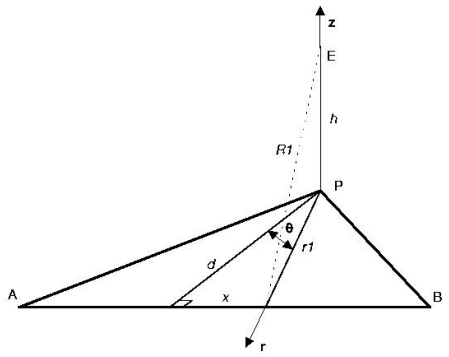

Figure 3: Triangle in polar coordinate system, d is the distance between point P and edge AB

reduced. The convergence behavior of the integration over the whole domain and over the two sub-domains is shown in figure 5. It is clear that the piece-wise scheme uses fewer quadrature points, or has higher accuracy if only a small number of quadrature points are used. Unfortunately, this is not appreciated in [4] and a small number (24) of quadrature points are used for the integration over the whole domain. Since the lower the frequency, the smaller the damping factor in complex wave number k, hence the higher the peak of the integrand $g(x)$, the formulation in [4] has a low frequency problem.

4. Using Normal Derivative to Reduce the Condition Number

At very low frequency, $G_1(\vec{r},\vec{r'})$ in equation (6) is almost the same as $G_0(\vec{r},\vec{r'})$ in equation (7). Therefore, equation (1) is very similar to equation (2), particularly for a single-conductor example, where S and S_k are the same. Therefore, the resulting system matrix will become ill-conditioned at low frequencies. If an iterative method is used to solve such an ill-conditioned linear system, the convergence will be slow.

We have developed a new formulation based on replacing equation (1) with the normal derivative of Green's second identity, and this reduces the condition number of the linear system. In the following, we give a brief derivation.

If we take the normal derivative of the equation (1), we have

$$\frac{\partial}{\partial n(\vec{r})}\int_{S_k} d\vec{r'} G_1(\vec{r},\vec{r'})\frac{\partial \vec{E}(\vec{r'})}{\partial n(\vec{r'})} -$$

$$\frac{\partial}{\partial n(\vec{r})}\int_{S_k} d\vec{r'}\frac{\partial G_1(\vec{r},\vec{r'})}{\partial n(\vec{r'})}\vec{E}(\vec{r'}) = \frac{1}{2}\frac{\partial}{\partial n(\vec{r})}\vec{E}(\vec{r}). \qquad (17)$$

Now the integral operators in equation (17) are different from those in equation (2). Hence the system matrix is not ill-conditioned at low frequencies any more. It should be noted that the unknowns in equation(17) are still E_x, E_y, E_z, $\frac{\partial Ex}{\partial n}$, $\frac{\partial Ey}{\partial n}$ and $\frac{\partial Ez}{\partial n}$. No extra unknowns are involved. So we could simply replace equation (1) with equation (17) and keep equation (2-5), generating an improved surface integral formulation. However, a hyper-singular term appears in equation (17). In this paper, this hyper-singular integral

$$I_4(\vec{r}) = \frac{\partial}{\partial n(\vec{r})}\int_{P_i} d\vec{r'}\frac{\partial G(\vec{r},\vec{r'})}{\partial n(\vec{r'})} \qquad (18)$$

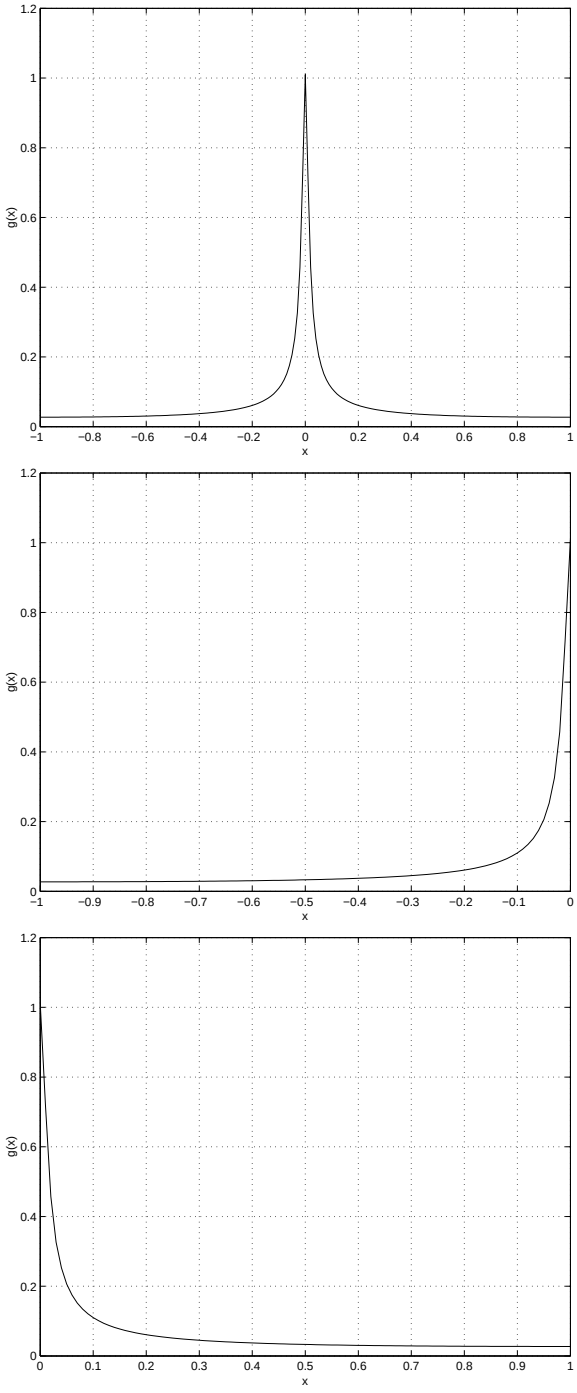

Figure 4: Distribution of the integrand, the top figure is the distribution of the original integrand, the middle and the bottom figure are the left and right part of the top figure

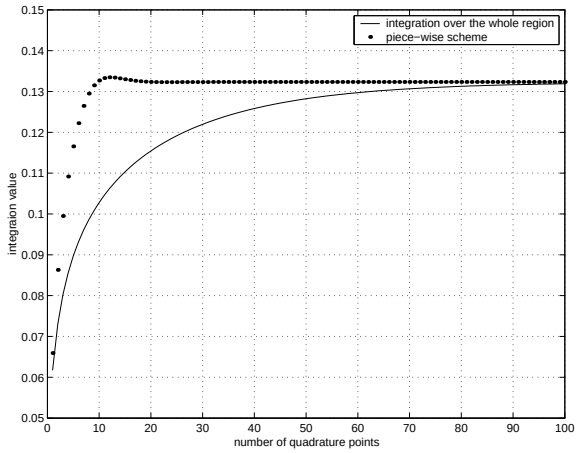

Figure 5: convergence behavior of different schemes

is calculated by using finite-differences to approximate the normal derivative outside the integral.

5. Numerical Results

In this section, we present some computation results using the improved surface integral formualtion and the piece-wise quadrature scheme. In order to compare with the magnetoquasistatic analysis program FastHenry, all the examples were analyzed magnetoquasistaticly. The formulation used still follows equations (1)-(5), though equation (3) is eliminated and the charge in equation (5) is set to be zero. We first use a simple ring structure to validate our panel integration scheme as analytical formulas exist for the inductance of a ring [6]. We then use our improved formulation to perform the analysis of a spiral inductor with or without a semiconductor substrate ground plane and a multipin connector, and compare the results to the public domain program FastHenry [2]. The sparse pre-conditioner matrix used in this paper is constructed by ignoring the interaction between panels in equation (1-3) and using equation (4) and (5) directly.

5.1 Ring

The ring is 10*mm* in radius, with a square cross section of the size 0.5*mm* by 0.5*mm*. The conductivity is that of the copper, which is 5.8e7. The low frequency inductance calculated using the formula in [6] is 48.89 nH. The results obtained by using FastHenry and the formulation proposed in [3, 4] enhanced with the piece-wise quadrature scheme proposed in section 3 are shown in figure 6 and 7. The two results agree well. The number of filaments used by FastHenry is 960, 3840 and 15360, respectively. The surface formualtion only uses 992 panels across the entire frequency range. It should be noted that the inductance obtained with the surface formulation is very close to 48.89nH in the low frequency range. This suggests that the low frequency problem reported in [4] has been eliminated without using the linearization technique proposed therein. Also, at high frequency, the resistance scales to the square root of frequency and the inductance drops a little. This suggests that the skin-effect has been well captured. So this ring example does validate our panel integration scheme.

5.2 Spiral inductor

The improved surface formulation generates a dense matrix. So it can not be used for analyzing complicated structures directly. It could be combined with an accelerated iterative method that allows for general Green's function, such as the Precorrected-FFT algorithm [7] or the hierarchal SVD [8]. Since we have not yet implemented an accelerated ver-

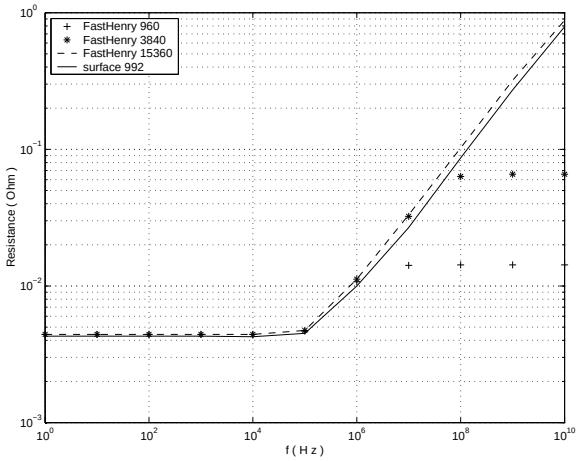

Figure 6: Resistance of a ring

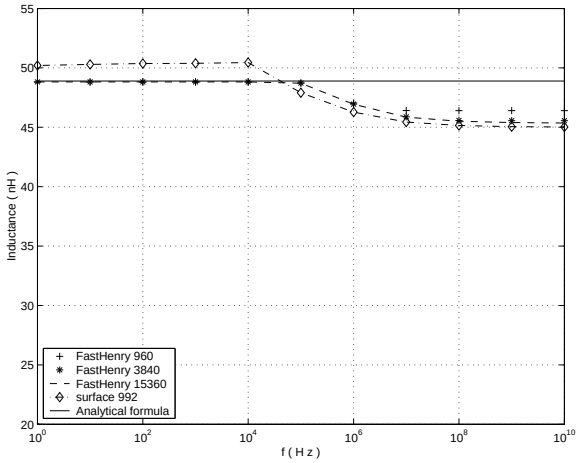

Figure 7: Inductance of a ring

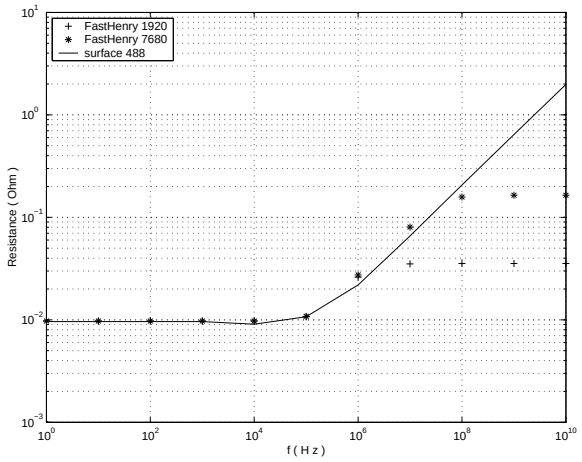

Figure 8: Resistance of a spiral

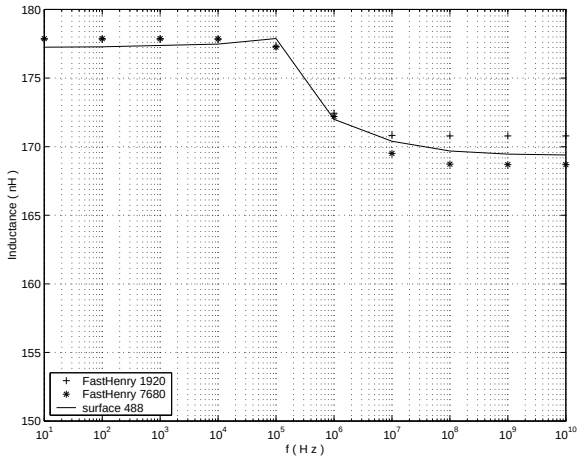

Figure 9: Inductance of a spiral

sion of our formulation, in this section we try to use a relatively coarse discretization to analyze a spiral inductor with or without a semiconductor ground plane to validate our improved surface integral formulation. And since an inductor with ground plane is a relatively complicated structure, we also use this example to show that the improved formualtion indeed converges faster than the formulation in [3].

The inner radius of the spiral is 10mm. Its cross section is a square of the size 0.5mm by 0.5mm, and the spacing between two succesive revolutions is 0.5mm. The spiral has two revolutions. The computed resistance and inductance agree well with those obtained with FastHenry, as shown in figure 8 and 9. Again, it is worth mentioning that FastHenry does not capture the skin-effect at high frequency due to the fixed number of filaments. On the other hand, with a fixed number of panels, the improved surface formualtion has well captured the skin-effect. This validates our improved surface formulation.

To test the convergence of the iterative method used to solve the linear system, we use the same spiral and add a semiconductor ground plane. The size of the ground plane is 42 by 42 mm. Its thickness is 1mm. Its conductivity is 0.005 that of the copper. We use the improved formulation and the formulation in [3] to analyze this structure at frequency point 1Hz. The number of unknowns is 2534. The residual of the GMRES versus the iterations for both formulations is shown in figure 10. It is clear that the improved formulation converges much faster.

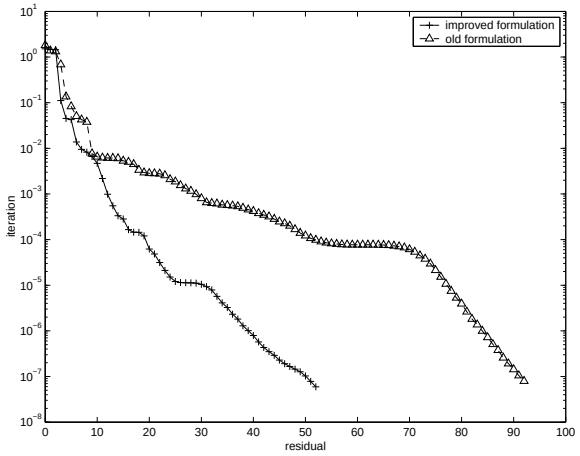

Figure 10: GMRES residual in old and improved formulation, a spiral inductor over ground plane

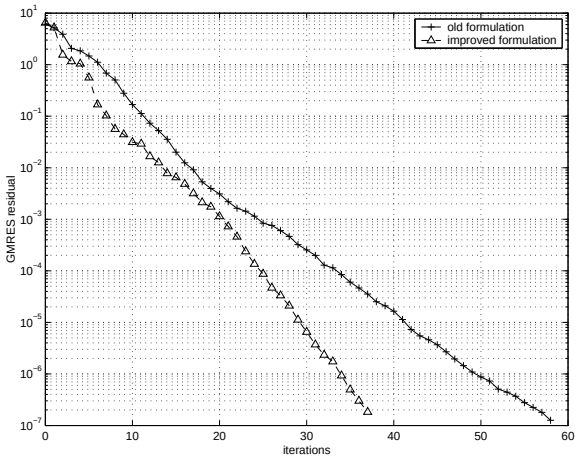

Figure 11: GMRES residual in old and improved formulation, a multipin connector

5.3 Multipin connector

To further test the convergence behavior of the improved formualtion, we also use it to analyze a three-pin connector. The number of panels is 544, and the number of unknowns is 3808. We again choose the frequency point to be 1Hz to see how the improved formulation speeds up the convergence at low frequency. The residual of the GMRES versus the iterations for both formulations is shown in figure 11. We can see that the number of iterations has been reduced significantly.

6. Conclusions

By taking the normal derivative of one of the equations in an existing surface integral formulation, we have reduced the condition number of this formulation. Numerical analysis of a spiral inductor over ground plane example shows that the number of GMRES iterations could be reduced by as much as one half. We have also proposed a piece-wise integration scheme to improve the accuracy of the panel integration in the surface formulation. Using this scheme, we have shown that the low frequency problem reported before actually does not exist. Therefore, the linearization technique used to eliminate this problem is unnecessary.

7. References

[1] K. Nabors and J. White, “FASTCAP: A multipole-accelerated 3-D capacitance extraction program,” *IEEE Trans. on Computer-Aided Design*, vol. 10, pp. 1447–1459, November 1991.

[2] M. Kamon, M. J. Tsuk, and J. White, “Fasthenry: A multipole-accelerated 3-D inductance extraction program,” *IEEE Transactions on Microwave Theory and Techniques*, vol. 42, no. 9, pp. 1750–1758, September 1994.

[3] J. Wang and J. K. White, “A wide frequency range surface integral formualtion for 3d rlc extraction,” *International Conference on Computer Aided-Design*, 1999.

[4] Junfeng Wang, *A new surface integral formulation of EMQS impedance extraction for 3-D structures*, Ph.D. thesis MIT EECS Department, 1999.

[5] J. L. Hess and A. M. O. Smith, “Calculation of potential flow about arbitrary bodies,” *Progress in Aeronautical Science*, pp. 1–138, 1966.

[6] Frederick Warren Grover, *Inductance calculations, working formulas and tables*, Govt. Print. Off., New York, NY, 1946.

[7] J. R. Phillips and J. K. White, “A precorrected-FFT method for electrostatic analysis of complicated 3D structures,” *IEEE Trans. Computer-Aided Design*, pp. 1059–1072, 1997.

[8] S. Kapur and J. Zhao, “A fast method of moments solver for efficient parameter extraction of mcms,” 34^{th} *ACM/IEEE Design Automation Conference*, pp. 141–146, 1997.